

Universal manuscript template for Optica Publishing Group journals

1. Abstract

2 Lorem ipsum ~ 100 words

3 2. Introduction

4 IR spectroscopy has seen significant interest and application in bio-imaging because it provides a
5 chemical fingerprint of underlying samples in a label-free way [1]. However, although the most
6 relevant chemical information can be gathered in the mid-infrared ($\sim 3 - 12 \mu\text{m}$), slow signal
7 acquisition is often a limiting factor, whose trade-off can keep it from competing with label-based
8 fluorescence microscopy.

9 Fig. 1 attempts to visualize the significant developments that have been made in mid-infrared
10 hyperspectral imaging over roughly the last two decades. Experiments are mapped onto the
11 two important metrics of spectra acquisition speed, which captures the rate at which spectra
12 are gathered, and optical bandwidth, which captures the breadth of chemical content that can
13 be observed. The two variables are plotted against each other, since a significant difficulty lies
14 in achieving both metrics simultaneously. For a better one to one comparison, the acquisition
15 speeds listed for experiments that use focal plane arrays have been normalized to that of an
16 analogous point scanning experiment.
17

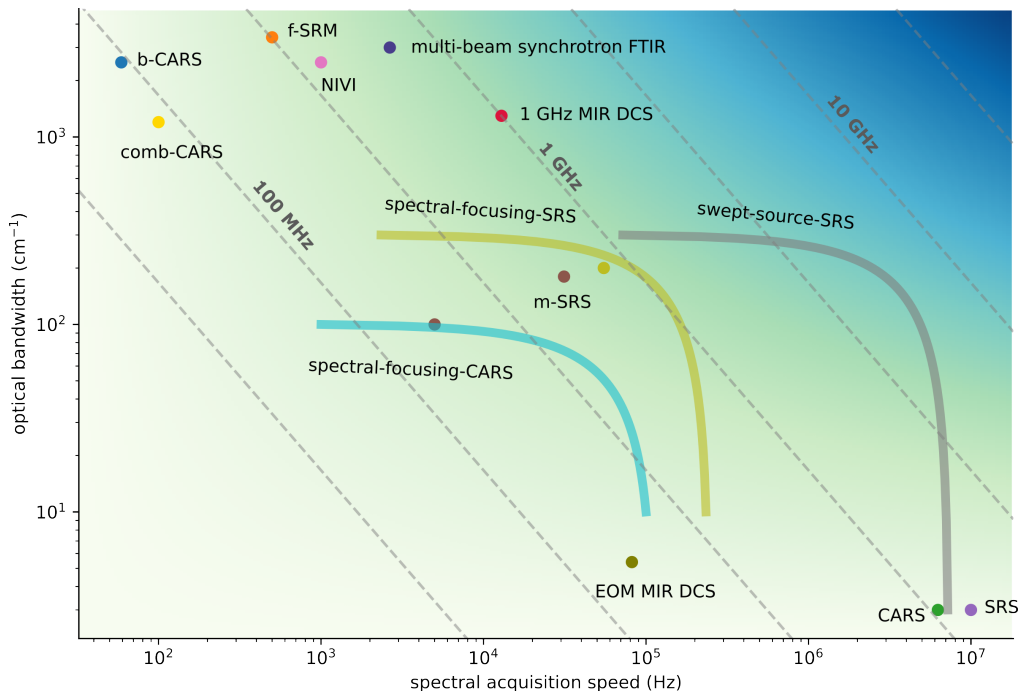


Fig. 1. Performance map of mid-infrared hyperspectral imaging. Broadband CARS (b-CARS) [2], femtosecond Stimulated Raman Microscopy (f-SRM) [3], in-vivo video rate CARS [4], in-vivo video rate SRS [5], multiplexed SRS (m-SRS) [6, 7], nonlinear interferometric vibrational imaging (NIVI) [8], swept-source SRS [9], spectral-focusing SRS [10], spectral-focusing CARS [11], spectral-focusing SRS [12], comb-CARS [13], multi-beam synchrotron FTIR [14], electro-optic modulator comb MIR DCS [15]

19 A few of the most notable experiments have utilized coherent Raman spectro-imaging, where
 20 in-vivo video-rate speeds have been demonstrated in the mid-infrared [4, 5]. Whereas initial
 21 demonstrations were over a narrow bandwidth ($\sim 3 \text{ cm}^{-1}$), broad bandwidths at high acquisition
 22 speeds have been demonstrated using rapidly rotating polygonal mirror scanners [12, 16]. However,
 23 the stated metrics are only possible with the strong Raman absorption cross-sections around
 24 2900 cm^{-1} , which precludes Raman spectroscopy-based platforms from achieving the same
 25 performance in the fingerprint region at longer wavelengths.

26 Conversely, Fourier transform spectroscopy (FTS) and quantum cascade laser (QCL) based
 27 imaging are attractive due to their broad applicability across the mid to long wavelength infrared.
 28 The high absorption cross-sections can also alleviate the need for operation at powers close to
 29 sample-damage thresholds, a concern that is applicable to biological samples. In this category,
 30 FTS spectrometers coupled to broadband and bright sources such as synchrotron facilities have
 31 set the state of the art for the combination of spectral bandwidth and speed [14]. The coupling of
 32 broadband synchrotron light into a microscope requires the active stabilization of a beam bundle.
 33 However, a widely accessible imaging method would benefit from having a simple and table
 34 top setup. QCL lasers are attractive due to their direct emission in the mid-infrared and small
 35 footprint, although their performance is best leveraged in narrowband applications. Tunable QCL
 36 packages consisting of multiple QCL chips combined into one device [17] can nominally reach
 37 broad spectral coverage, but struggle to reach noise figures comparable to platforms based on
 38 mode-locked lasers.

More recently, dual-comb spectroscopy (DCS) in the frequency comb community has become
 a popular platform, due to its improved stability and speed when compared to classical FTS [18].
 In this modality, the interference of two frequency combs maps a Nyquist band from the optical
 domain down into the RF. One of the most important considerations in DCS is the direct trade-off
 between the frequency resolution/repetition rate f_r and the size of the optical Nyquist window
 $\Delta\nu$:

$$\Delta\nu = \frac{f_r^2}{2\Delta f_r} \quad (1)$$

39 where Δf_r is the interferogram acquisition rate equal to the difference of the two laser repetition
 40 rates. The diagonal dashed lines in Fig. 1., show the $f_r^2/2$ trade-off between resolvable bandwidth
 41 and acquisition speed in DCS for different repetition rates. Evidently, when broad absorption
 42 features allow for coarse resolution, the highest repetition rates are desired. However, in order
 43 to reach sufficient power per comb tooth, in practice the pulse energy required for nonlinear
 44 frequency down-conversion from the near-infrared sets an upper limit on the obtainable repetition
 45 rate. In this work, we utilize a set of recently developed 1-GHz mid-infrared frequency combs [19]
 46 to integrate a dual-comb spectrometer with a confocal microscope. We capitalize on the high
 47 repetition rate by fully filling the third Nyquist band (2595cm^{-1} – 3890cm^{-1} at $\Delta f_r = 12.86\text{kHz}$).
 48 The system is among the fastest performers in the class of spectrometers covering over 1000
 49 cm^{-1} with high spectral resolution in the mid-infrared.

50 However, pointing to the dashed line in the upper right corner of Fig. 1, in order to achieve the
 51 ultimate goal of label-free broadband video-rate imaging, we note that the ideal DCS platform
 52 would operate with repetition rates of 10 GHz or higher. Such systems would likely require either
 53 high-power amplifiers or a nanophotonic design capable of generating equivalent bandwidths in
 54 the mid-infrared with pump pulse energies around 100 pJ.

55 3. Experiment

56 With long-term stability in mind, a single-branch intra-pulse difference frequency generation
 57 (DFG) design is used to generate light in the mid-infrared.

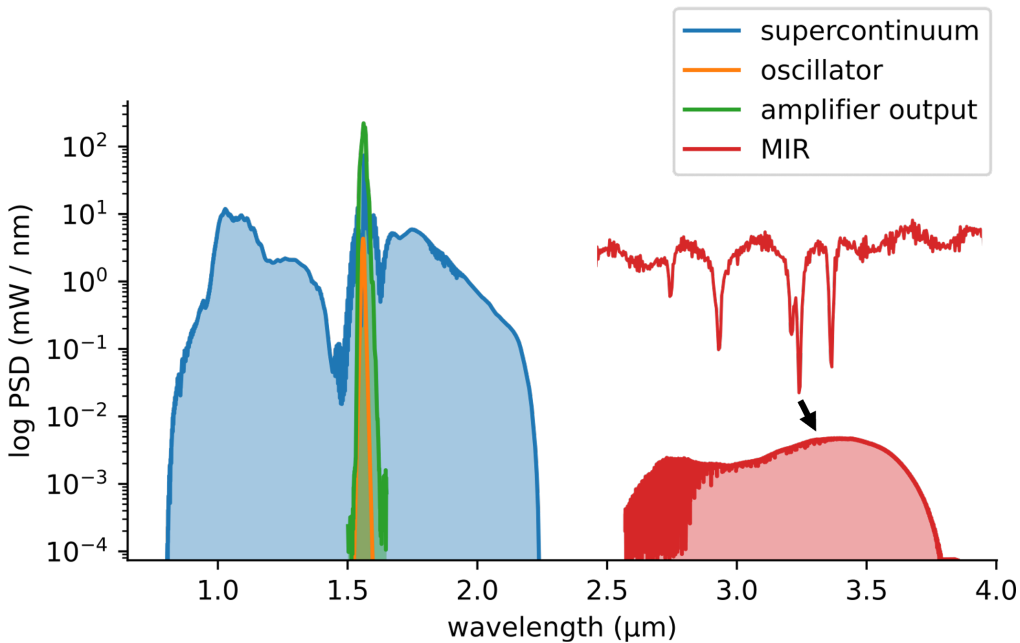


Fig. 2. 1 GHz MIR Frequency Comb. The spectral evolution through successive stages of the system: oscillator → chirped-pulse amplifier → few-cycle supercontinuum generation → MIR frequency down conversion. The inset shows a zoom in of waterlines that are resolved when using the full 1 GHz frequency resolution.

58 Shown in Fig. 2, to compensate for the low conversion efficiency of the single-branch design,
 59 octave spanning few cycle NIR pulses generated via soliton self-compression in anomalous
 60 dispersion highly nonlinear fiber are used to drive the nonlinear frequency down conversion to
 61 the mid-infrared. Although coverage of the 6-12 μm wavelength region can be achieved for one
 62 laser system, due to the lack of nonlinear crystals in this work more widely available lithium
 63 niobate is used to cover the 3 - 5 μm wavelength window.

64 Two 1-GHz mid-infrared frequency combs are generated and coupled into InF_3 single-mode
 65 fiber for delivery to the experiment, where the output beam is collimated with a two inch off-axis
 66 parabolic mirror. A reflective confocal microscope with 0.58 NA is used to image the beam
 67 onto a glass slide ($\sim 3.8 \mu\text{m}$ pixel size). The transmitted signal is focused onto a high-speed
 68 MCT detector, whose AC coupled port is digitized at 1 GS/s using an FPGA. The data is
 69 streamed concurrently from the card memory into PC RAM for real-time analysis, such that the
 70 card-memory does not limit the data volume.

71 4. Results

72 5. DCS Imaging Speed

Regardless of the imaging method, the final determination of imaging speed is given by the time needed to reach sufficient SNR at each pixel. Specifically for DCS microscopy, the target SNR and frequency resolution sets the pixel dwell time. In DCS, the absorbance noise σ scales with the frequency resolution and number of averaged spectra N_{avg} according to [20]:

$$\sigma \propto \frac{N}{\sqrt{N_{\text{avg}}}} \quad (2)$$

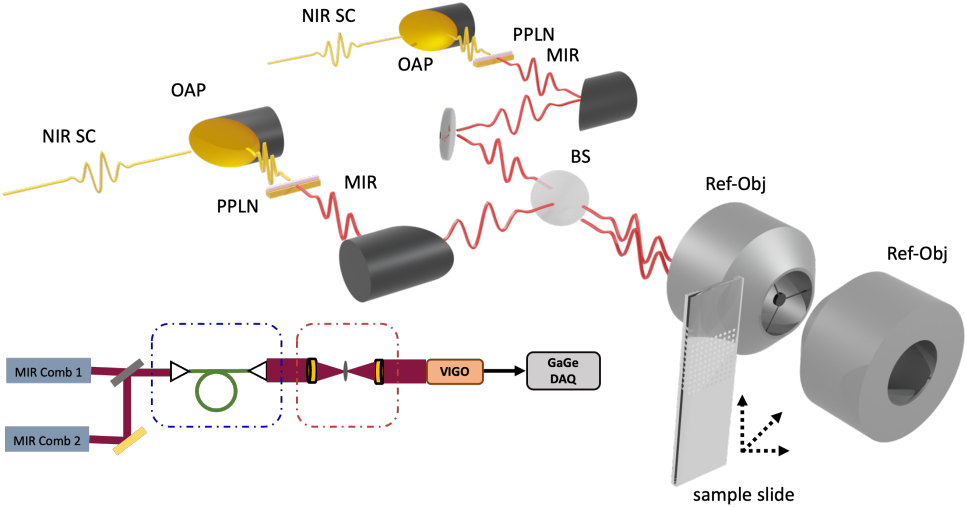


Fig. 3. Experimental Setup. Two mid-infrared frequency combs generated through intra-pulse difference frequency generation are passed collinearly through a confocal microscope. Hyperspectral images are collected by raster scanning the sample slide. The transmitted signal is collected and digitized in a high-speed MCT mid-infrared detector and FPGA.

73 where N is the number of frequency bins. This scaling rule is shown in Fig. 6. (c-d),, where it
 74 is observed to match the experimentally measured absorbance noise. The two-variable map in
 75 Fig. 6. (d). should apply more generally to to any DCS point scanning microscopy, but with the
 76 time axis scaled accordingly to the repetition rate.

77 Shown in Fig. 6. (a),, a baseline for 1 GHz DCS is that a 1000 cm^{-1} Nyquist window can be
 78 covered with $\sim 17 \text{ kHz}$ spectra acquisition speed, which is a two order magnitude improvement
 79 over well-established 100 MHz MIR laser sources. In Fig. 6. (b),, a single-shot spectrum ($77 \mu\text{s}$)
 80 at 1-GHz has low signal to noise, but can be averaged to high SNR in two seconds ($>25,000$
 81 spectra). However, a high SNR can be achieved in $\sim 39 \text{ ms}$ at 500 averages if the interferograms
 82 are apodized to 100 GHz ($\sim 3.33 \text{ cm}^{-1}$). The SNR as a function of averaging time and frequency
 83 resolution is shown in Fig. 6. (c-d);; the absorbance noise always averages down according to
 84 $1/\sqrt{N_{\text{avg}}}$, but with coarser resolution resulting in a directly proportional overall noise reduction.

85 References

- 86 1. M. J. Baker, J. Trevisan, P. Bassan, R. Bhargava, H. J. Butler, K. M. Dorling, P. R. Fielden, S. W. Fogarty, N. J.
 87 Fullwood, K. A. Heys, C. Hughes, P. Lasch, P. L. Martin-Hirsch, B. Obinaju, G. D. Sockalingum, J. Sulé-Suso, R. J.
 88 Strong, M. J. Walsh, B. R. Wood, P. Gardner, and F. L. Martin, "Using Fourier transform IR spectroscopy to analyze
 89 biological materials," *Nat. Protoc.* **9**, 1771–1791 (2014).
- 90 2. T. W. Kee and M. T. Cicerone, "Simple approach to one-laser, broadband coherent anti-Stokes Raman scattering
 91 microscopy," *Opt. Lett.* **29**, 2701 (2004).
- 92 3. E. Ploetz, S. Laimgruber, S. Berner, W. Zinth, and P. Gilch, "Femtosecond stimulated Raman microscopy," *Appl.
 93 Phys. B* **87**, 389–393 (2007).
- 94 4. C. L. Evans, E. O. Potma, M. Puoris'haag, D. Côté, C. P. Lin, and X. S. Xie, "Chemical imaging of tissue *in vivo* with
 95 video-rate coherent anti-Stokes Raman scattering microscopy," *Proc. National Acad. Sci.* **102**, 16807–16812 (2005).
- 96 5. B. G. Saar, C. W. Freudiger, J. Reichman, C. M. Stanley, G. R. Holtom, and X. S. Xie, "Video-Rate Molecular
 97 Imaging in Vivo with Stimulated Raman Scattering," *Science* **330**, 1368–1370 (2010).
- 98 6. D. Fu, F.-K. Lu, X. Zhang, C. Freudiger, D. R. Pernik, G. Holtom, and X. S. Xie, "Quantitative Chemical Imaging
 99 with Multiplex Stimulated Raman Scattering Microscopy," *J. Am. Chem. Soc.* **134**, 3623–3626 (2012).

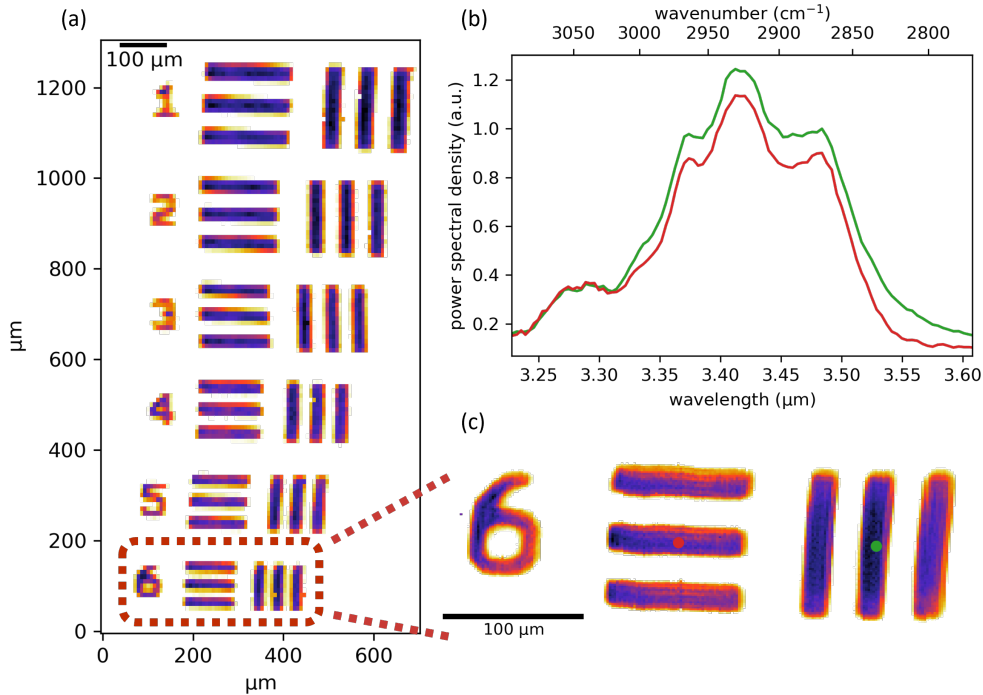


Fig. 4. Caption

- 100 7. C.-S. Liao, M. N. Slipchenko, P. Wang, J. Li, S.-Y. Lee, R. A. Oglesbee, and J.-X. Cheng, "Microsecond scale
101 vibrational spectroscopic imaging by multiplex stimulated Raman scattering microscopy," *Light. Sci. & Appl.* **4**,
102 e265–e265 (2015).
- 103 8. P. D. Chowdary, Z. Jiang, E. J. Chaney, W. A. Benalcazar, D. L. Marks, M. Gruebele, and S. A. Boppart, "Molecular
104 Histopathology by Spectrally Reconstructed Nonlinear Interferometric Vibrational Imaging," *Cancer Res.* **70**,
105 9562–9569 (2010).
- 106 9. Y. Ozeki, W. Umemura, Y. Otsuka, S. Satoh, H. Hashimoto, K. Sumimura, N. Nishizawa, K. Fukui, and K. Itoh,
107 "High-speed molecular spectral imaging of tissue with stimulated Raman scattering," *Nat. Photonics* **6**, 845–851
108 (2012).
- 109 10. D. Fu, G. Holtom, C. Freudiger, X. Zhang, and X. S. Xie, "Hyperspectral Imaging with Stimulated Raman Scattering
110 by Chirped Femtosecond Lasers," *The J. Phys. Chem. B* **117**, 4634–4640 (2013).
- 111 11. C. Di Napoli, I. Pope, F. Masia, P. Watson, W. Langbein, and P. Borri, "Hyperspectral and differential CARS
112 microscopy for quantitative chemical imaging in human adipocytes," *Biomed. Opt. Express* **5**, 1378 (2014).
- 113 12. H. Lin, H. J. Lee, N. Tague, J.-B. Lugagne, C. Zong, F. Deng, J. Shin, L. Tian, W. Wong, M. J. Dunlop, and J.-X.
114 Cheng, "Microsecond fingerprint stimulated Raman spectroscopic imaging by ultrafast tuning and spatial-spectral
115 learning," *Nat. Commun.* **12**, 3052 (2021).
- 116 13. T. Ideguchi, S. Holzner, B. Bernhardt, G. Guelachvili, N. Picqué, and T. W. Hänsch, "Coherent Raman spectro-imaging
117 with laser frequency combs," *Nature* **502**, 355–358 (2013).
- 118 14. M. J. Nasse, M. J. Walsh, E. C. Mattson, R. Reiningher, A. Kajdacsy-Balla, V. Macias, R. Bhargava, and C. J.
119 Hirschmugl, "High-resolution Fourier-transform infrared chemical imaging with multiple synchrotron beams," *Nat. Methods* **8**, 413–416 (2011).
- 120 15. F. Ullah Khan, G. Guarnizo, and P. Martín-Mateos, "Direct hyperspectral dual-comb gas imaging in the mid-infrared,"
121 *Opt. Lett.* **45**, 5335 (2020).
- 122 16. M. Tamamitsu, Y. Sakaki, T. Nakamura, G. K. Podagatlapalli, T. Ideguchi, and K. Goda, "Ultrafast broadband
123 Fourier-transform CARS spectroscopy at 50,000 spectra/s enabled by a scanning Fourier-domain delay line," *Vib.
124 Spectrosc.* **91**, 163–169 (2017).
- 125 17. K. Yeh, S. Kenkel, J.-N. Liu, and R. Bhargava, "Fast Infrared Chemical Imaging with a Quantum Cascade Laser,"
126 *Anal. Chem.* **87**, 485–493 (2015).
- 127 18. I. Coddington, N. Newbury, and W. Swann, "Dual-comb spectroscopy," *Optica* **3**, 414 (2016).
- 128 19. N. Hoghooghi, S. Xing, P. Chang, D. Lesko, A. Lind, G. Rieker, and S. Diddams, "Broadband 1-GHz mid-infrared

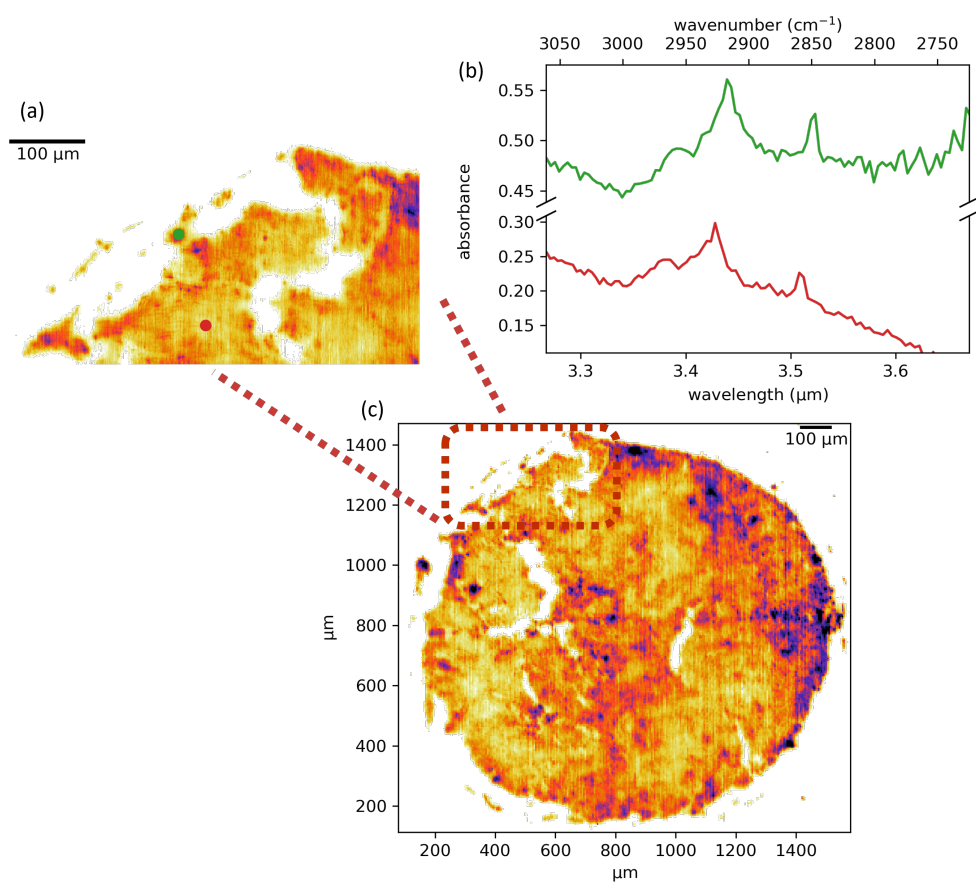


Fig. 5. Caption

- 130 frequency comb," Light. Sci. & Appl. **11**, 264 (2022).
 131 20. N. R. Newbury, I. Coddington, and W. Swann, "Sensitivity of coherent dual-comb spectroscopy," Opt. Express **18**,
 132 7929 (2010).

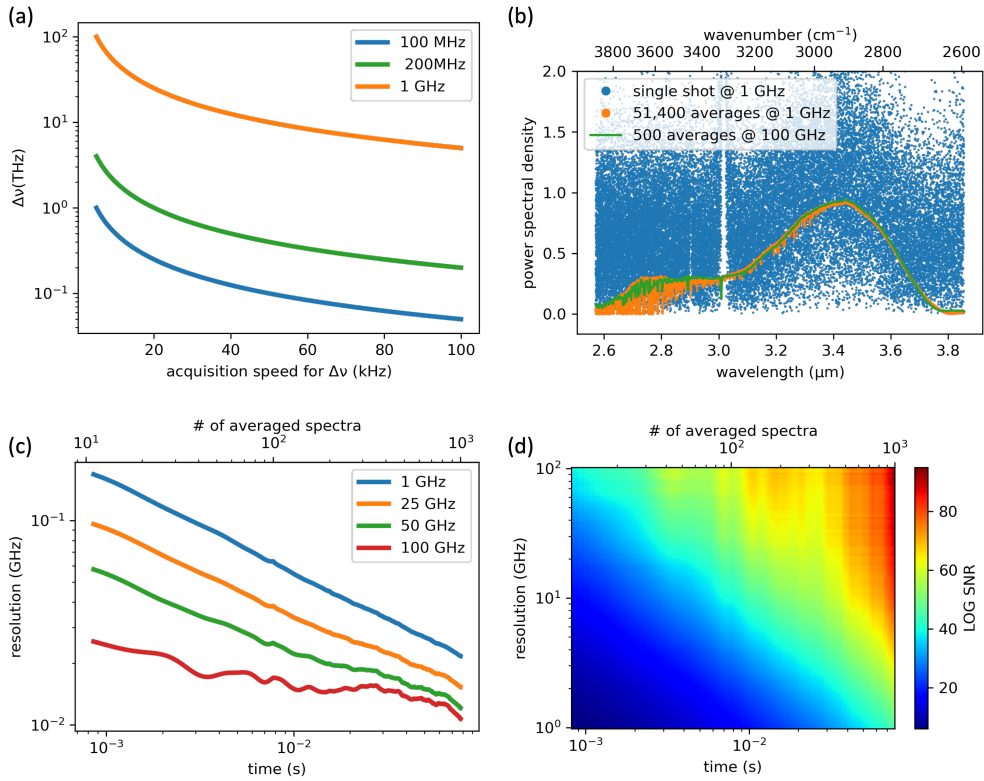


Fig. 6. Summary of DCS Imaging Speed. (a) The size of the optical Nyquist window plotted against acquisition speed (Δf_r) for different repetition rates. (b) DCS spectrum taken at different averaging times and frequency resolution/apodization windows. (c) The spectra's SNR follow the scaling of Eq. 2, with an example of the 2D parameter space (d) mapped out for the 1-GHz system.